Table 1. Summary of Patients' Demographic Data

Case	Age	Sex	Pathology	Level for Osteotomy	Symptom	Operative Plan
1	63	M	HCC metastasis	T12	None	*En bloc* tumor resection
2	31	M	Chondrosarcoma	L4	Low back pain	*En bloc* tumor resection
3	25	F	Fibrosarcoma	T4 and T6	Back pain	Total *en bloc* spondylectomy
4	35	M	Ankylosing spondylitis	L3	Back pain and kyphosis	Posterior closing wedge osteotomy

HCC indicates hepatocellular carcinoma.

such as the lateral decubitus position, pedicle screws were placed under the assistance of the navigation system. The precise localization of the starting point and the direction of vertebral osteotomy were confirmed by the navigation system. The surgeon can check the real-time localization and the direction of the pointer tip on several 2D and 3D views on the computer screen.

Spinal osteotomy was performed using an osteotome with step-by-step confirmation of the tip position of the osteotome by the navigation system. At the same time, the navigation system provided useful anatomic information during the blind maneuver around the neurovascular structures behind the tumor or close to the vertebral body, which decreased the risk for neurovascular injury. In cases involving combined osteotomy from both the anterior and posterior approaches, it was important to keep the reference frame on the spinous process for navigating during the posterior and anterior procedures.

Case Studies

Case 1. The patient was a 63-year-old man with metastasis of hepatocellular carcinoma without symptoms. The original lesions of the hepatocellular carcinoma were resolved completely after nonoperative treatments such as transcatheter arterial embolization and chemotherapy. An asymptomatic solitary metastatic lesion adjacent to the T12 vertebral body was recognized on a magnetic resonance (MR) image at the 2-year follow-up after resolution of the hepatic tumor (Figure 1). The general condition of the patient was good. Other metastatic lesions were not recognized in whole-body CT, scintigraphy, or ^{18}F-fluorodeoxyglucose positron emission tomography, and curative treatment for the metastatic lesion was advocated.

En bloc tumor resection to include the lateral part of the T12 vertebral body, proximal part of the 12th rib, and surrounding soft tissue through a single posterior approach was scheduled. Under general anesthesia, the patient was placed on the operation table in a right lateral decubitus position. Pedicle screws were placed from right T11 to L1 and left T11 to L1 without difficulty under the assistance of the navigation system. The assistance of the navigation system was useful for precise pedicle screw placement in the unfamiliar operative position. After the left-side hemilaminectomy and the total excision of the facet joints from T11 to L1, the left 11th and 12th spinal roots were cut under ligation. A spinal osteotomy was performed using an osteotome with step-by-step confirmation of the tip position of the osteotome by the navigation system (Figure 2A). Another skin incision was made along the left 11th rib. After the excision of the 11th rib, the anterior part of the tumor was exposed through extrapleural and retroperitoneal approaches. At this point, it was decided to cut a portion of the 12th rib with a safety margin under the guidance of the navigation system. After mapping out the starting point of the vertebral osteotomy from the anterior side, the anterior and ending points of the posterior vertebral osteotomy were connected (Figure 2B). After blunt dissection of the paravertebral muscle with a safety margin under the guidance of the navigation system, the lateral aspect of the vertebral body, tumor, and proximal portion of the 12th rib were removed *en bloc* without tumor exposure. Interbody fusions using a titanium cage with harvested 11th rib grafting and posterior instrumentation were completed.

The operating time was 377 minutes, and the estimated intraoperative blood loss was 1620 mL. The postoperative course was uneventful. The patient was allowed to ambulate beginning on the first day after surgery. Postoperative CT revealed the precise osteotomy and instrumentation (Figure 3). Pathologic analysis confirmed *en bloc* tumor resection without exposure. At 1 year after the surgery, the patient reported no complaints, there was no local recurrence, and the spinal construct was solid radiologically.

Case 2. The patient was a 31-year-old man who complained of lower back pain caused by a huge tumor at L4. Diagnosis of chondrosarcoma was confirmed by a preoperative open biopsy at another institute. CT and MR imaging showed a huge bone tumor possibly originating from the transverse process of L4 and extending into the paravertebral muscles (Figure 4). Preoperative systemic evaluation confirmed the localized lesion

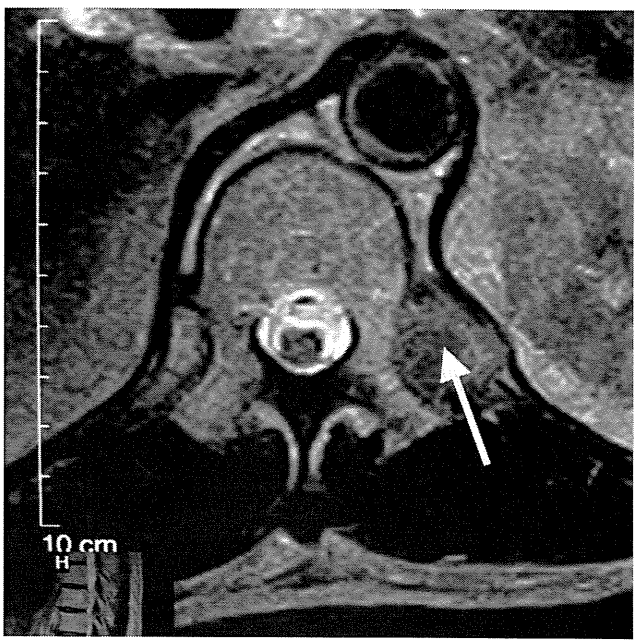

Figure 1. Case 1. Preoperative MR axial image demonstrating the solitary metastatic lesion adjacent to the T12 vertebral body. The arrow indicates the tumor.

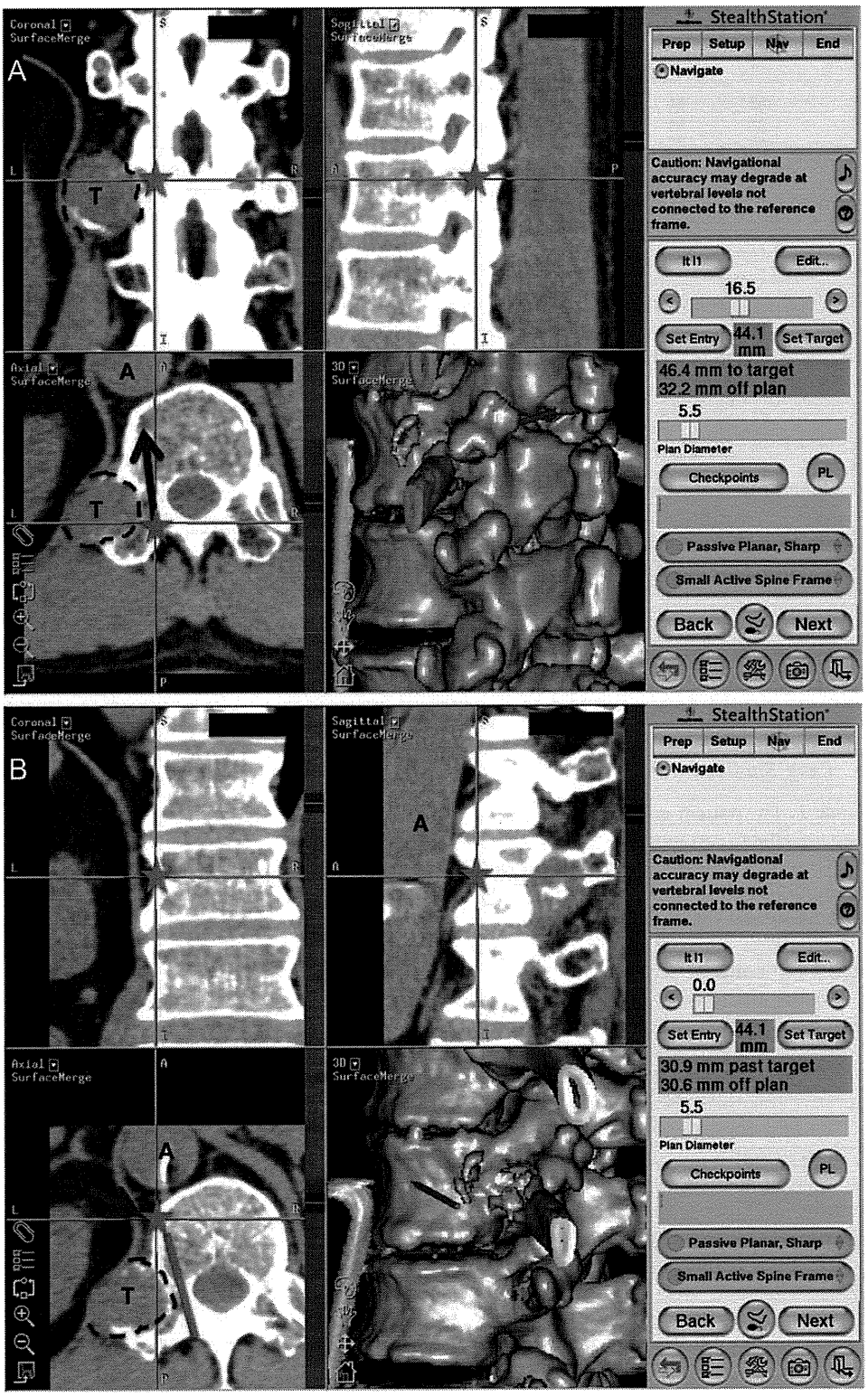

Figure 2. Case 1. The navigation system's views provide 3-dimensional, coronal, parasagittal, and axial images in conjunction with the actual instrument tip image. **A,** Pointer tip mapping of the starting point of the osteotomy from the posterior direction (asterisk). The arrow indicates the planned osteotomy from the posterior direction. The dotted line indicates the tumor margin. **B,** Pointer tip mapping of the starting point of the osteotomy from the anterior direction (asterisk). The arrow indicates the direction of the osteotomy from the anterior direction, which connects to the ending point of the osteotomy from the posterior direction. T indicates tumor; A, aorta.

without metastasis. A curative operation was planned to involve an *en bloc* tumor resection combined with the right half of the L4 vertebral body. Computer-assisted spinal osteotomy and *en bloc* tumor resection were performed through the combined anterior and posterior exposure as described in case 1 (Figure 5).

The right L2–L4 nerve roots were involved in the huge tumor and were killed. The osteotomized vertebral body, huge tumor, and paravertebral muscle were removed *en bloc* without tumor exposure. Spinal reconstruction with a titanium cage with autogenous iliac crest bone graft and anteroposterior instrumentation from L2 to S1 was performed. An incidental dural tear was repaired successfully. The operating time was 999 minutes, and the estimated intraoperative blood loss was 7000 mL. Postoperative CT demonstrated complete resection of the tumor and a precise osteotomy of the right half of the vertebral body and reconstruction using the titanium cage (Figure 4). Pathologic analysis revealed complete excision of the

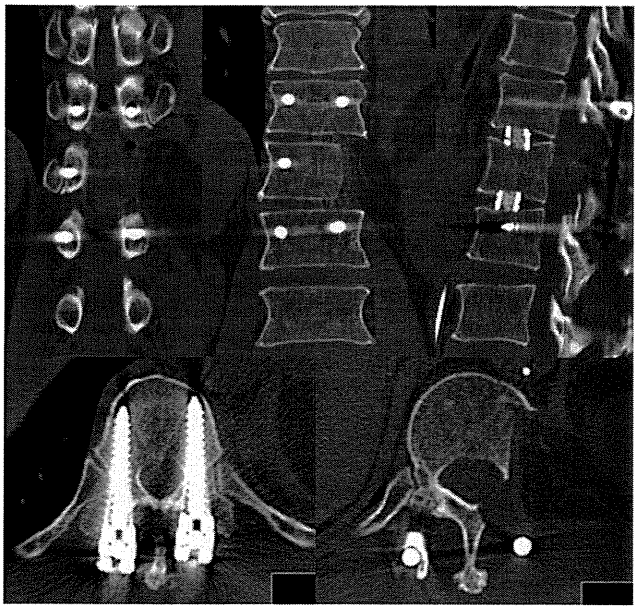

Figure 3. Case 1. Postoperative CT images demonstrating the precise osteotomy, *en bloc* tumor excision, and accurate pedicle screw placement.

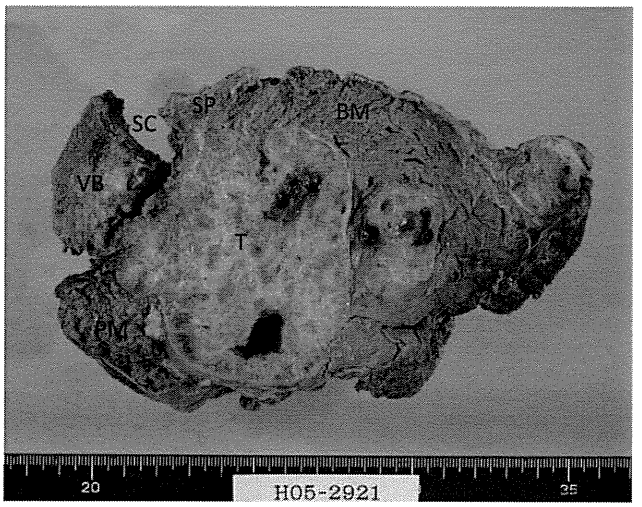

Figure 5. Case 2. Photograph of cross section of the *en bloc* specimen after removal. VB indicates vertebral body; T, paravertebral tumor; SC, spinal canal; SP, spinous process; BM, back muscle; PM, psoas muscle.

huge tumor without exposure on the osteotomy line. Although right leg paresis occurred as a result of the intentional nerve root sacrifice, the patient could ambulate with one cane. Bony union was achieved through the cage 1 year after the surgery (Figure 6). Although no local recurrence was observed at the 2-year follow-up, the patient died from lung metastasis 3 years after the surgery.

Case 3. The patient was a 25-year-old woman who complained of severe back pain caused by a pathologic fracture at T5. Diagnosis of fibrosarcoma was defined by a preoperative needle biopsy. CT and MR imaging demonstrated a pathologic fracture and epidural tumor extension from caudal T4 to cranial T6, which compressed the spinal cord severely (Figure 7). Preoperative whole-body examination confirmed a solitary lesion without metastasis. A total *en bloc* spondylectomy from caudal T4 to cranial T6 was scheduled. A computer-assisted spinal osteotomy using a T-saw and total *en bloc* spondylectomy were performed through a single posterior exposure. The safety margin of the spinal osteotomy and the relationship with the surrounding neurovascular structures were confirmed at each step of the operation using the navigation system. The navigation system provided important anatomic information during the blind maneuver around the anterior aspect of the vertebral body.

After the *en bloc* spondylectomy, spinal reconstruction with a titanium cage with an autogenous iliac crest bone graft and posterior instrumentation from T3 to T8 were performed. The operating time was 495 minutes, and the estimated intraoperative blood loss was 1640 mL. Pathologic analysis revealed complete resection of the tumor without exposure. A postop-

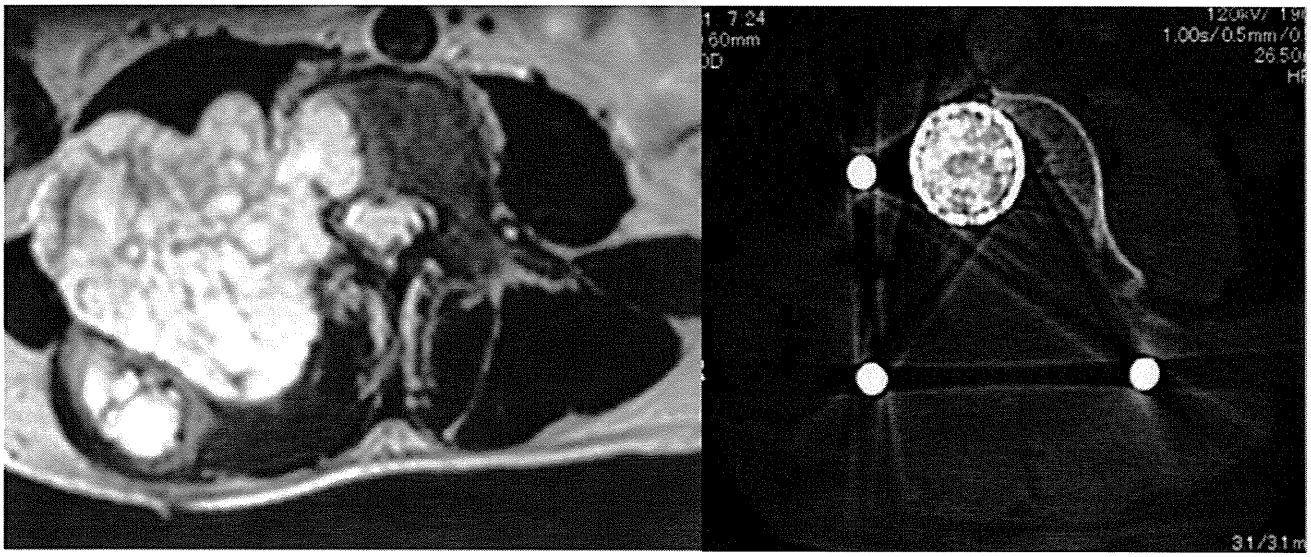

Figure 4. Case 2. Comparison of preoperative MR axial image (left) and postoperative (right) CT axial image. The images demonstrate the precise *en bloc* excision of a large tumor by spinal osteotomy and reconstruction using a titanium mesh cage with an autogenous bone graft.

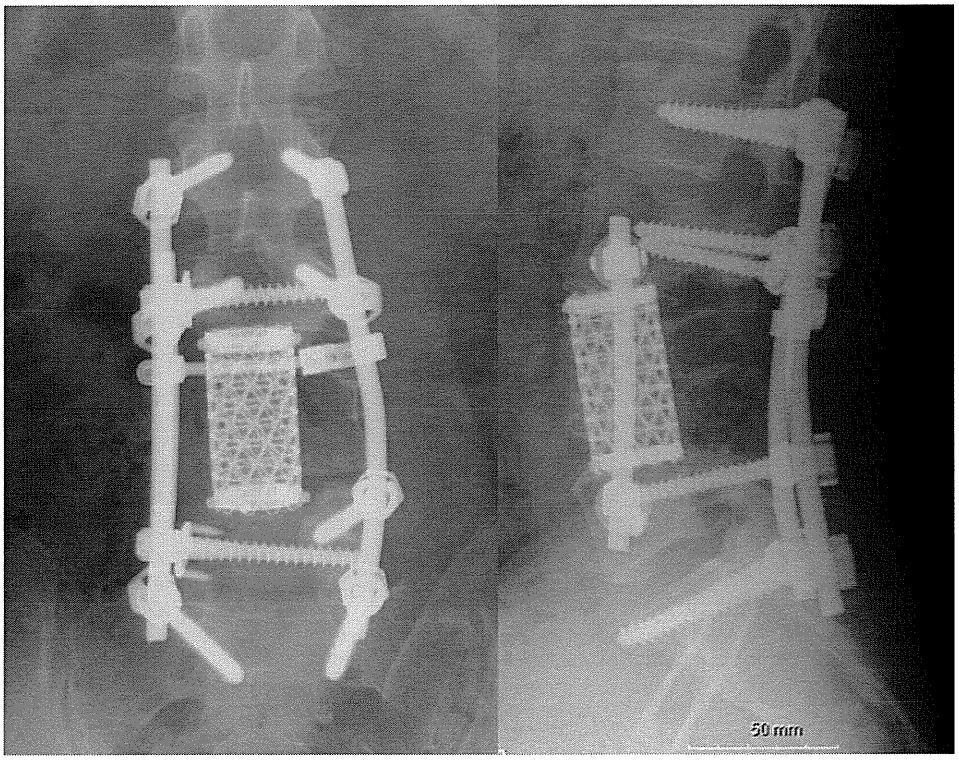

Figure 6. Case 2. Anteroposterior and lateral radiographs at the 1-year postoperative follow-up showing spinal reconstruction after *en bloc* tumor resection and solid bony union.

erative CT demonstrated the precise osteotomy and spinal reconstruction using the titanium cage (Figure 7). The postoperative course was uneventful, and the patient underwent adjuvant chemotherapy. One year after surgery, radiologic examination showed good bony union through the cage and no local recurrence (Figure 8).

Case 4. The patient was a 35-year-old man who complained of back pain and a severe kyphotic posture that prevented him from looking forward and maintaining the supine position, which restricted his daily activities severely. Ankylosing spondylitis was diagnosed as "bamboo spine," and the patient was HLA-B27 positive and had elevated C-reactive protein concentration. Kyphosis was 77° caused by the combination of 48° at the thoracic spine (T1–T12) and 29° at the lumbar spine (L1–L5) (Figure 9). A C7 plumb line was shifted 27.9 cm anteriorly to the sacral promontory, and the chin-brow vertical angle (CBVA) was 54° (Figure 10A).[16] We scheduled a 45° posterior-closing wedge spinal osteotomy at the L3 vertebra and posterior instrumentation from T12 to L5. The degree of spinal osteotomy and the relationship with surrounding neurovascular structures were confirmed at each step of the operation using the navigation system. A temporary rod was attached to the pedicle screws across to the osteotomy to avoid sudden movement. The osteotomized site was closed successfully using a bending maneuver on a flexible operating table and gradual compression with instrumentation. Postoperative lateral radiograph and CT revealed a 44° osteotomy (Figure 9), which corrected the lumbar lordosis to 15°, the anterior shift of the C7 plumb line to 5.4 cm, and the CBVA to 9° (Figure 10B). The operating time was 421 minutes, and the estimated intraoperative blood loss was 536 mL. After the operation, the patient

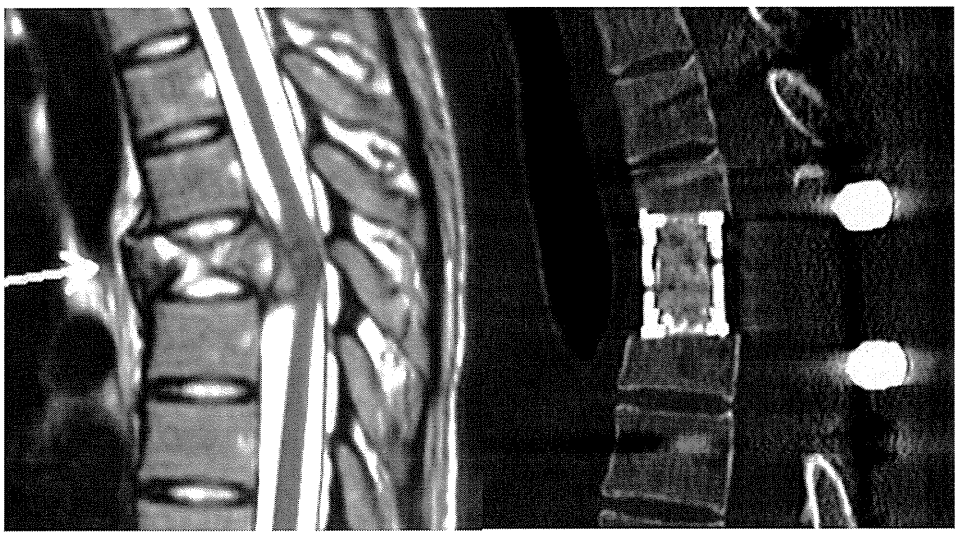

Figure 7. Case 3. Comparison of preoperative MR sagittal image (left) and postoperative (right) CT sagittal image. The images demonstrate the precise total *en bloc* spondylectomy from caudal T4 to cranial T6 by spinal osteotomy and reconstruction using a titanium mesh cage with an autogenous bone graft.

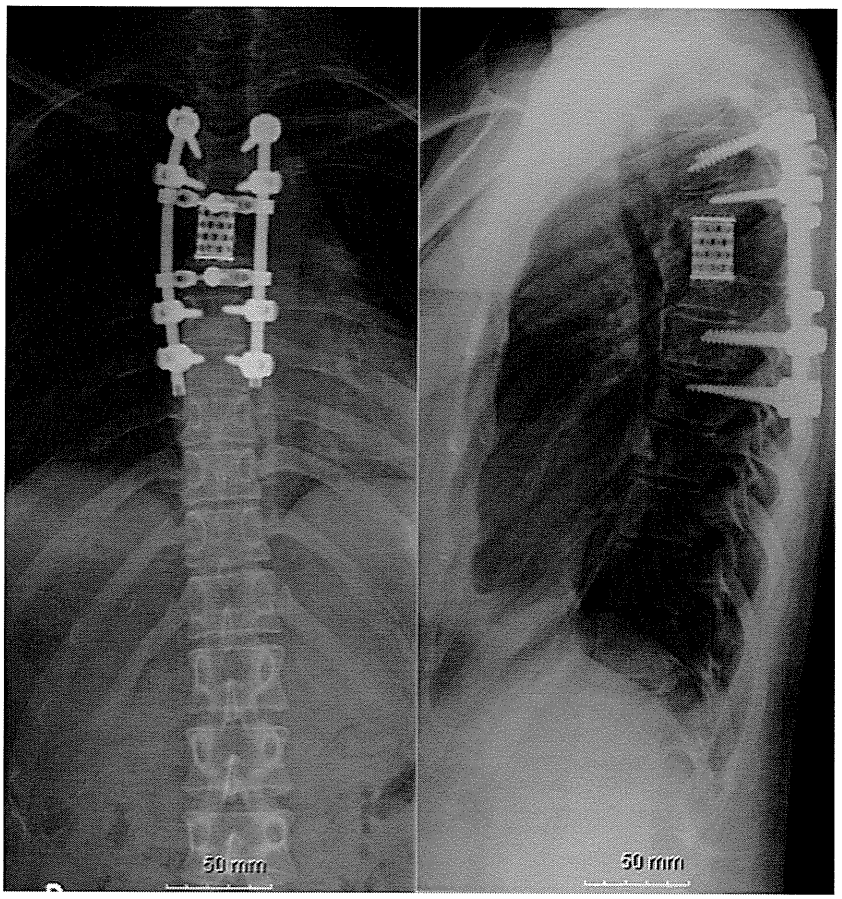

Figure 8. Case 3. Anteroposterior and lateral radiograph of the thoracic spine at the 1-year postoperative follow-up showing restoration of the sagittal alignment after *en bloc* tumor resection and solid bony union.

could look forward and maintain a supine position, and his back pain resolved. Successful bony union at the osteotomized site was achieved 6 months after the operation, and sagittal alignment was well maintained at the 1-year follow-up.

■ Results and Discussion

In all 4 patients, 3D spinal osteotomy was performed successfully. The computer-assisted navigation system was useful for mapping the osteotomy site and surrounding tissues intraoperatively in every patient. Postoperative radiograph and CT confirmed the precise osteotomy, implant placement, and deformity correction according to the preoperative plan. Pathologic analysis also showed *en bloc* tumor resection without tumor exposure on the osteotomy line in all 3 tumor cases. The results of the operative procedure are summarized in Table 2.

Computer-assisted surgery, using a CT-based navigation system, has been introduced successfully to facilitate highly accurate surgical procedures in spinal surgery. The operative field and preoperative images are combined by registration, or integration, of the preoperative imaging methods within the surgical environment. The accuracy and usefulness of a navigation system in the placement of pedicle screws are recognized and have been discussed. Numerous comparative studies have demonstrated the increased accuracy of pedicle screw placement for several spinal disorders including cervical and scoliosis surgery.[17,18]

Other applications of the navigation system include the excision of spinal pathologies, including osteoid osteoma, hemangioma, chordoma, ossification of the posterior longitudinal ligament, and ossification of the ligamentum flavum.[3–9] The navigation system provides the information needed to excise the lesion completely without causing neurovascular injury to the surrounding tissues.

We think other good candidates for navigation surgery are 3D deformity correction and *en bloc* tumor resection, which require a precise osteotomy and excision according to the preoperative planning. In such complex anatomic pathologies, even skillful and experienced surgeons can lose the localization and orientation during the operation, which can lead to poor surgical results and complications. Spinal osteotomy is a complex surgery involving the wide resection of a malignant tumor *en bloc* or correction of a fixed spinal deformity. The problems for conventional spinal osteotomy include the blind maneuver around the spinal cord, nerve root, and major vessels, and the potential for incorrect or insufficient osteotomy, tumor exposure during incorrect osteotomy, insufficient correction of a spinal deformity, or nonunion after the corrective osteotomy. A rigid spinal deformity such as ankylosing spondylitis does not have a compensatory mechanism, and precise osteotomy and correction are required. We performed a precise osteotomy for each

Figure 9. Case 4. Comparison of preoperative (left) and postoperative (right) CT sagittal images. The images demonstrate the precise osteotomy at L3 and correction of the ankylosing spondylitis deformity.

patient according to preoperative planning, and the follow-up showed that successful postoperative sagittal alignment and early bony union were achieved. In patients with a solitary malignant tumor in the spine, *en bloc* resection with a safety margin, such as a total *en bloc* spondylectomy, is mandatory to provide a curative treatment.[19–21]

In all our tumor patients, total resection with a safety margin was the best procedure. In general, total resection for such lesions requires combined anterior and posterior approaches, and a very invasive operation. In patients 1 and 3, using the navigation system allowed the operations to be performed in single stages without the need to change the patient's position, which decreased the surgi-

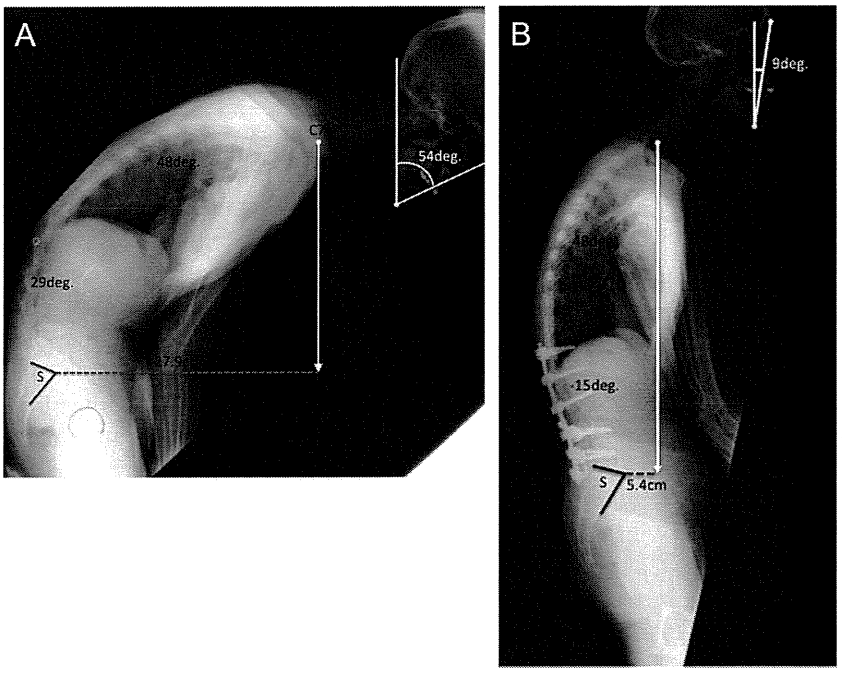

Figure 10. Case 4. Comparison of preoperative (**A**) and postoperative (**B**) full-length lateral radiographs. Lumbar lordosis, anterior shift of the C7 plumb line, and CBVA were corrected from 29° of kyphosis, 27.9 cm, and 54° to −15° of kyphosis, 5.4 cm, and 9°, respectively.

Table 2. Summary of Postoperative Clinical Data

Case	Operative Time (min)	Blood Loss (mL)	% EBV*	Operative Procedure	Complications
1	377	1620	32.2	*En bloc* tumor resection, Posterior interbody fusion (T11–L1)	None
2	999	7000	156.6	*En bloc* tumor resection, Anteroposterior spinal fusion (L2–S)	Dural tear and right leg paresis†
3	495	1640	54.8	Total *en bloc* spondylectomy, Posterior spinal fusion (T3–T8)	None
4	421	536	13.0	Closing wedge osteotomy, Posterior spinal fusion (T12–L5)	None

Average blood volume = 75 mL/kg in adult men, 65 mL/kg in adult women.
% EBV = blood loss/EBV [times] 100.
*EBV (estimated blood volume) = weight (kg) [times] average blood volume.
†Right leg paresis caused by intentional right L2–L4 nerve root sacrifice.

cal invasiveness and decreased the operating time. The navigation system allows the optimal anteroposterior, mediolateral, and rostral-caudal trajectories of the osteotomy selected in the virtual model to be replicated intraoperatively. Thus, a safe 3D osteotomy can be performed with the optimal amount and orientation of correction, which increases the safety of the neural and vascular structures. In addition, we estimate that both the patient and surgeon receive less radiation exposure than if standard fluoroscopy is used.

Another major advantage of navigation surgery is the feasibility of virtual surgery and practicing the operative plan before surgery. The surgeon can experience virtual surgery several times on the computer screen using 2D- and 3D-reconstructed CT images, which provide the important anatomic information to the surgeon before the operation, and facilitate the safety and accuracy of the operation in the real operative theater.

The disadvantage of existing CT-based navigation systems is the difficulty in navigating the anatomically flat structures such as the anterior spine and postlaminectomy spine. In such situations, setting the reference frame and accomplishing the surface registration are difficult. The usefulness of image-assisted surgery using intraoperative CT for multioperated complex deformity surgery was reported recently.[14] Such new technology will provide a less invasive, safer, and more accurate surgery. In addition, the instrumented spine is difficult to navigate because of the artifact related to the metal implants. In the clinical arena, salvage surgeries are often required for such complex pathologies, and development of novel navigation systems is required to solve such problems.

Because this is a technical note, and the sample size and follow-up periods were limited, it was difficult to compare the obvious advantages of computer-assisted surgery with conventional fluoroscopy-guided surgery in terms of the long-term clinically relevant outcomes. The use of a computer-assisted navigation system will help ensure the safety and efficacy of a complex 3D spinal osteotomy.

■ Key Points

- The surgical technique and usefulness of computer-assisted surgery for spinal osteotomy are presented.
- Four complex cases, including 3 solitary malignant spinal tumors and 1 spinal kyphotic deformity of ankylosing spondylitis, were treated surgically using a computer-assisted navigation system.
- The navigation system provided useful real-time information to the surgeon during the osteotomy surgery; this information included the precise localization and orientation of the tumor or deformity.

References

1. Kosmopoulos V, Schizas C. Pedicle screw placement accuracy: a meta-analysis. *Spine* 2007;32:E111–20.
2. Rajasekaran S, Vidyadhara S, Ramesh P, et al. Randomized clinical study to compare the accuracy of navigated and non-navigated thoracic pedicle screws in deformity correction surgeries. *Spine* 2007;32:E56–64.
3. Arand M, Hartwig E, Kinzl L, et al. Spinal navigation in tumor surgery of the thoracic spine: first clinical results. *Clin Orthop Relat Res* 2002;398:211–8.
4. Neo M, Asato R, Honda K, et al. Transmaxillary and transmandibular approach to a C1 chordoma. *Spine* 2007;32:E236–9.
5. Rajasekaran S, Vijay K, Shetty AP. Intraoperative Iso-C three-dimensional navigation in excision of spinal osteoid osteomas. *Spine* 2008;33:E25–9.
6. Sakanishi H, Hoshi K, Nakajima S, et al. Vertebral hemangioma compressing the thoracic spinal cord: application of computer-aided navigation and intraoperative spinal sonography for surgery through anterior and posterior approaches. *J Orthop Sci* 2006;11:294–7.
7. Seichi A, Nakajima S, Takeshita K, et al. Image-guided resection for thoracic ossification of the ligamentum flavum. *J Neurosurg* 2003;99(suppl 1):60–3.
8. Seichi A, Takeshita K, Kawaguchi H, et al. Image-guided surgery for thoracic ossification of the posterior longitudinal ligament. Technical note. *J Neurosurg Spine* 2005;3:165–8.
9. Van Royen BJ, Baayen JC, Pijpers R, et al. Osteoid osteoma of the spine: a novel technique using combined computer-assisted and gamma probe-guided high-speed intralesional drill excision. *Spine* 2005;30:369–73.
10. Stulberg SD, Beng PL, Sarin V. Computer-assisted navigation in total knee replacement: results of an initial experience in thirty-five patients. *J Bone Joint Surg Am* 2002;84:90–8.
11. Gregg RK, Matthew SA, Smith EB, et al. Total knee arthroplasty using computer-assisted navigation in patients with deformities of the femur and tibia. *J Arthroplasty* 2006;21:284–8.
12. Jackson DW, Warkentine B. Technical aspects of computer-assisted opening wedge high tibial osteotomy. *J Knee Surg* 2007;20:134–41.
13. Keppler P, Gebhard F, Grutzner PA, et al. Computer aided high tibial open wedge osteotomy. *Injury* 2004;35(suppl 1):S-A68–78.
14. Metz LN, Burch S. Computer-assisted surgical planning and image-guided surgical navigation in refractory adult scoliosis surgery case report and review of the literature. *Spine* 2008;33:E287–92.
15. Ohmori K, Kawaguchi Y, Kanamori M, et al. Image-guided anterior thoracolumbar corpectomy: a report of three cases. *Spine* 2001;26:1197–201.
16. Suk KS, Kim KT, Lee SH, et al. Significance of chin-brow vertical angle in correction of kyphotic deformity of ankylosing spondylitis patients. *Spine* 2003;28:2001–5.

17. Kotani Y, Abumi K, Ito M, et al. Improved accuracy of computer-assisted cervical pedicle screw insertion. *J Neurosurg* 2003;99(suppl 3):257–63.
18. Kotani Y, Abumi K, Ito M, et al. Accuracy analysis of pedicle screw placement in posterior scoliosis surgery comparison between conventional fluoroscopic and computer-assisted technique. *Spine* 2007;32:1543–50.
19. Melcher I, Disch AC, Khodadadyan-Klostermann C, et al. Primary malignant bone tumors and solitary metastases of the thoracolumbar spine: results by management with total en bloc spondylectomy. *Eur Spine J* 2007;16: 1193–202.
20. Sakaura H, Hosono N, Mukai Y, et al. Outcome of total en bloc spondylectomy for solitary metastasis of thoracolumbar spine. *J Spinal Disord Tech* 2004;17:297–300.
21. Tomita K, Kawahara N, Baba H, et al. Total en bloc spondylectomy for solitary spinal metastases. *Int Orthop* 1994;18:291–8.

SPINE Volume 35, Number 11, pp E452–E457

Advantages of the Paraspinal Muscle Splitting Approach in Comparison With Conventional Midline Approach for S1 Pedicle Screw Placement

Masato Ota, MD, Masashi Neo, MD, PhD, Shunsuke Fujibayashi, MD, PhD, Mitsuru Takemoto, MD, PhD, and Takashi Nakamura, MD, PhD

Study Design. A retrospective comparative study of the S1 pedicle screw (S1PS) position obtained using 2 surgical approaches.

Objective. To determine whether the paraspinal approach leads to more medially oriented placement of the S1PS compared with the midline approach.

Summary of Background Data. To obtain a stronger as well as safer fixation of the S1PS, medially oriented screw placement is very important. However, no study has recommended a surgical approach to achieve this object.

Methods. The positions of 32 screws placed by the midline approach and 34 screws placed by the paraspinal approach were compared using postoperative computed tomography. The location of the bilateral common iliac veins (CIV) in relation to the S1PS tips was also analyzed to evaluate their safety.

Results. There was no statistical difference in screw insertion point regardless of the approach employed. However, in the paraspinal group the S1PS were placed with significantly greater medial direction and with longer screws. In addition, they pierced the anterior sacral cortex closer to the midline compared with the midline approach. Four left screws in the midline approach group made contact with the left CIV, whereas no screw in the paraspinal approach group lay adjacent to the CIV.

Conclusion. Our results demonstrate that the paraspinal approach for S1PS placement may be superior to the midline approach in terms of the medially oriented screw placement that is biomechanically stronger and less risky for the CIV.

Key words: sacral screw fixation, paraspinal approach, pedicle screw, complication, mechanical strength. **Spine 2010;35:E452–E457**

Pedicle screw fixation in the lumbar spine has been relatively successful, but S1 pedicle screw (S1PS) fixation remains a challenging clinical problem. Despite efforts to develop a stable S1PS fixation technique, a high incidence of instrumentation failure and pseudarthrosis continue to plague the procedure.[1,2] Problems of S1PS fixation, particularly with the placement of the S1PS without supplemental distal fixation, are attributable to not only biologic but also mechanical factors of the sacrum. These factors include low bone mineral density of the sacrum, difficulty in obtaining an appropriate direction of the S1PS, large cantilever bending forces being applied to the distal instrumentation, and the difficulty in access to, and visualization of, the starting point of the S1PS.[3] To overcome these disadvantages, alternative fixation techniques, such as posterior sacral fixation with iliac fixation, combination of S1PS with a sacral alar screw or hooks, or an S2PS have been proposed.[4] However, increasing the range of internal fixations may give rise to instrument-related complications, and fixations into the ilium may create disorders of the sacroiliac joint.[5]

It is essential, therefore, that techniques for the placement of S1PS to achieve ideal sacral purchase should be established. A variety of studies regarding biomechanical evaluations of S1PS orientation as well as screw purchase in the anterior sacral cortex have been investigated previously.[6–15] In particular, the S1PS orientation should be considered. Convergence of the PSs produces a triangulation effect that should substantially increase the pullout strength of a fully assembled construct. Barber *et al* verified that compared with those placed in parallel, paired PSs placed at 30 degrees of convergence in the lumbar spine sustained a statistically higher load at the threshold of loosening.[14] Furthermore, it is generally agreed that medially oriented placement of the S1PS provides greater stability than either straight-ahead or laterally oriented positions, because the mean bone mineral density in the central region of the sacrum was found to be approximately 30% to 60% higher than in the alar region.[12,13] Peretti *et al*, in their cadaveric study showed that S1PS with an inward obliquity of 10 degrees had 43% greater resistance to pullout forces than those with a straight-ahead position.[7] Similarly, Zheng *et al* clarified that the insertion torque of medially directed S1PS was 42% to 101% higher than that of laterally directed S1PS.[13] Thus, it seems that medially oriented S1PS placement is necessary to obtain a secure anchor to the sacrum.

Bicortical screw fixation also increases the mechanical strength of a S1PS.[10,13] In this case, however, knowledge of the neurovascular structures anterior to the sacrum is very important. Not only excessive penetration of the ventral sacral cortex but also far lateral screw penetration potentially carries greater risks to the neurovascular structures such as the iliac vessels and the lumbosacral

From the Department of Orthopaedic Surgery, Graduate School of Medicine, Kyoto University, Kyoto, Japan.
Acknowledgment date: August 4, 2009. Revision date: September 29, 2009. Acceptance date: November 3, 2009.
The device(s)/drug(s) is/are FDA-approved or approved by corresponding national agency for this indication.
No funds were received in support of this work. No benefits in any form have been or will be received from a commercial party related directly or indirectly to the subject of this manuscript.
Address correspondence and reprint requests to Masato Ota, MD, Department of Orthopaedic Surgery, Graduate School of Medicine, Kyoto University, 54 Kawahara-cho, Shogoin, Sakyo-ku, Kyoto 606-8507, Japan; E-mail: otamasa@kuhp.kyoto-u.ac.jp

trunk.[16–19] Although, fortunately, a fatal case has never been reported, Ergur *et al* reported that injuries of the lumbosacral trunk could cause neurologic deficit or chronic pain.[18] To avoid these complications, an adequate medial orientation of the S1PS is necessary.

Considering the combination of biomechanical advantages and anatomic safety, a S1PS placement as medially oriented as possible is desirable. However, no study has yet addressed the best surgical approach to permit medially oriented placement of the S1PS screws. The purpose of this study was to investigate whether a paraspinal muscle-splitting approach leads to more medially oriented placement of the S1PS compared with the conventional midline approach. In addition, we attempted to examine the location of the common iliac vein (CIV) to assess the safety of anterior sacral structures.

■ Materials and Methods

Patient Population

A total of 68 S1PS were placed in 34 patients with degenerative disorders who underwent lumbosacral fixation at our institution between May 2001 and May 2008, and who were examined with postoperative computed tomography (CT) imaging. Patients with infections, tumors, or previous lumbosacral surgery were excluded from this study. To compare 2 surgical approaches for S1PS placement, the subjects were classified into 2 groups. Of the 68 screws, 32 S1PS in 16 patients were inserted by the conventional midline approach up to June 2005, whereas 36 S1PS in 18 patients were inserted using the paraspinal muscle-splitting approach described by Wiltse *et al*[20] from July 2005 onward. To harvest massive bone graft, the bilateral posterior superior iliac spine was resected in only 1 case with the paraspinal approach, and it was excluded from this study. Consequently, the midline approach group consisted of 32 S1PS in 16 patients and the paraspinal approach group consisted of 34 S1PS in 17 patients.

The demographic characteristics of the patients in these groups including age, gender, preoperative diagnosis, fusion level, and surgical method for lumbosacral fusion are listed in Table 1. The original diagnoses in both groups were diverse lumbosacral degenerative disorders as shown in Table 1.

Table 1. Patient Demographic Data

	Midline Approach Group	Paraspinal Approach Group	*P*
No. patients	16	17	
No. S1 pedicle screws	32	34	
Mean age at surgery (±SD)	53.3 ± 20.6	46.6 ± 17.6	0.2639*
Gender (male/female) (% male)	10/6 (62.5)	12/5 (70.6)	0.6223†
Preoperative diagnosis (% of patients)			
Degenerative spondylolisthesis	5 (31.3)	2 (11.8)	
Isthmic spondylolisthesis	4 (25)	6 (35.3)	
Degenerative disc disease	2 (12.5)	3 (17.6)	
Recurrent disc hernia	3 (18.8)	2 (11.8)	
Intraforaminal disc hernia	1 (6.3)	2 (11.8)	
Other conditions	1 (6.3)	2 (11.8)	
Level of fusion (% of patients)			
One level (L5/S1)	11 (68.8)	15 (88.2)	
Two levels (L4–S1)	3 (18.8)	2 (11.8)	
Three levels (L3–S1)	1 (6.3)	0	
Four levels (L2–S1)	1 (6.3)	0	
Surgical method for L5/S1 fusion (% of patients)			
Transforaminal lumbar interbody fusion	10 (62.5)	16 (94.1)	
Posterior lumbar interbody fusion	6 (37.5)	1 (5.9)	

*Mann-Whitney *U* test.
†χ^2 for independence test.

Surgical Procedures for S1PS Placement

In both approaches, a midline posterior skin incision was made. In the midline approach, the deep fascia was incised in the middle, and the multifidus muscles were subsequently freed from spinous processes and lamina attachments to the lateral aspect of the L5/S1 facet joint by conventional techniques. However, in the paraspinal approach the paramedian fascial incisions were made in their correct place, which was usually located 2 to 3 cm lateral to the midline. After the natural cleavage plane of the anatomic intermuscular space between multifidus and longissimus muscles was identified, a muscle-splitting technique using blunt finger dissection between these muscles could be used to gain access to the lateral parts of the L5/S1 facet joint. In both approaches, our entrance point for the S1PS insertion was the inferolateral corner of the S1 superior articular process. Orientation of the screw axis was aimed as medially as possible to a sacral midline in the horizontal plane. The posterior superior iliac spine was not resected. In the sagittal plane, the sacral promontory was located under lateral fluoroscopic guidance. We aimed for secure fixation by pinching the screw tip between the anterior and superior cortices of the sacral promontory. However, when the surgeon wanted more secure fixation the anterior sacral cortex was carefully penetrated by a pedicle probe or an awl. To obtain a bicortical fixation of the screw, we chose a screw that was 0 to 5 mm longer than the measured depth to the anterior cortex. After the pathway was inspected with a sounder for any bone breaches, the S1PS was inserted with the identical trajectory.

All screws were placed by 1 of 3 senior authors or under their supervision. Eleven types of PS systems were used in this study. The selection of the PS type was at the surgeon's discretion.

Assessment Using CT

A postoperative CT scan was routinely performed within a few weeks of surgery for all patients to confirm whether the graft bone or interbody cages, as well as the PSs, had been implanted in the correct position. Three different types of CT scanner were used in this series: the Lemage Supreme (GE Yokogawa Medical Systems, Tokyo, Japan), HiSpeed QX/i (GE Yokogawa Medical Systems, Tokyo, Japan), and Aquilion64 (Toshiba Medical Systems, Tokyo, Japan). Horizontal slices along the S1PS axis were cut to a slice thickness of 2 to 3 mm and a slice interval of 2 to 3 mm in all cases. The best slice close to the center of the screw was selected to evaluate the position of the S1PS and the location of the CIV anterior to the sacrum on both sides, as follows.

First, we measured from the CT images for all 66 S1PS the distance from the anteroposterior sacral vertebral midline to the midpoint of the screw at the posterior cortical insertion point (IPD), the S1PS angle (PSA), which was defined as the angle between the screw axis and the midline, the S1PS length (PSL), which was defined as the distance between the screw midpoints at the IPD and the anterior cortical penetration point, and the distance from the midline to the lateral edge of

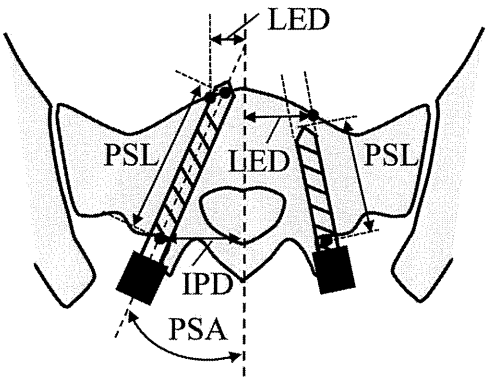

Figure 1. Illustration of the measurements made of the S1pedicle screw (S1PS) position. IPD indicates distance from the vertebral midline to the screw insertion point; PSA, S1PS angle; PSL, length of S1PS length within the sacral body; LED, distance from the midline to the lateral edge of the screw perforation at the anterior sacral cortex. The right side screw of the illustration shows the method of measurement of PSL and LED when the screw did not reach the anterior cortex.

the S1PS perforation of the anterior sacral cortex (LED) (Figure 1). When the S1PS did not reach the anterior sacral cortex, PSL was measured as the distance from the screw tip to the IPD. LED was also defined as the distance from the midline to the cross-point of the extension of the lateral edge of the screw and the anterior cortex as shown in Figure 1.

Second, to compare the anatomic locations of bilateral CIVs, the shortest distance from the midline to the CIV (MVD) and the shortest distance from anterior sacral cortex to the CIV (SVD) were measured (Figure 2). For these assessments, we decided on the correct position of the CIV after referring to several cranial CT images which were traced back to the level of divergence of the inferior vena cava. Only 26 screws (13 images) in the midline approach group and 30 screws (15 images) in the paraspinal approach group were eligible, because for 3 images in the former group and 2 in the latter it was difficult to precisely confirm the contour of the CIV. When the S1PS protruded anterior to the sacral anterior cortex we also measured for each group the number of screws that were situated <1 mm from the CIV.

All linear and angular parameters were measured with a precision of 0.5 mm and 0.5 degrees, as dictated by Centricity PACS system version 2.0 (GE healthcare, Milwaukee, WI). All records were retrospectively examined by the first author.

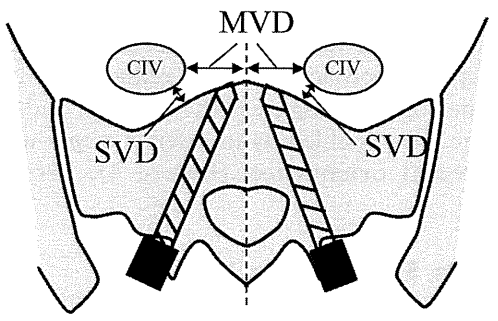

Figure 2. Illustration of measurements indicating the location of the right and left common iliac vein (CIV). MVD indicates the shortest distance from the midline to the CIV; SVD, the shortest distance from the anterior sacral cortex to the CIV.

Table 2. S1 Screw Position in the 2 Treatment Groups

	Midline Approach Group	Paraspinal Approach Group	*P*
No. S1 pedicle screws	32	34	
IPD (mm)	28.9 ± 2.18	30.1 ± 2.83	0.0867
PSA (degrees)	17.1 ± 6.82	23.7 ± 6.27	0.0002*
PSL (mm)	43.2 ± 5.12	46.5 ± 4.44	0.029*
LED (mm)	18.9 ± 4.86	13.9 ± 7.16	0.0017*

*$P < 0.05$.
IPD indicates distance from the vertebral midline to the screw insertion point; PSA, S1 pedicle screw angle; PSL, S1 pedicle screw length in the sacral body; LED, distance from the midline to the lateral edge of the screw at the anterior sacral cortex.

Statistical Analyses

The Mann-Whitney *U* test was performed to compare the nonparametric variables such as the S1 screw positions of the 2 groups and the CIV locations on right and left sides. The χ^2 for independence test was used for comparison of the frequencies. $P < 0.05$ was considered to be significant. All statistical analyses were performed using StatView software version 5.0 (SAS Institute Inc., Cary, NC).

■ Results

There were no significant differences in age and gender between the 2 treatment groups (Table 1). All 66 S1PS were fully contained within the cortical boundaries of the S1 pedicle and no screw was identified on CT evaluation to have breached the medial wall of the S1 pedicle. Screw diameters were 6.5 or 7.5 mm in both groups and no significant differences in screw diameters between the 2 groups were found ($P = 0.1055$). Twenty-one (65.6%) of 32 screws in the midline approach group penetrated the anterior sacral cortex by an average of 3.33 ± 1.86 mm whereas 18 (52.9%) of 34 screws in the paraspinal approach group penetrated by a mean of 4.11 ± 2.15 mm. Neither the number of penetrated screws nor their protruded length was significantly different between the 2 groups ($P = 0.2949$ and $P = 0.2312$, respectively).

The S1PS positions in the 2 groups, which were assessed by IPD, PSA, PSL, and LED, are summarized in Table 2. When the screw insertion point estimated by IPD was analyzed, there was no significant difference. In contrast, significant differences were found between the 2 treatment groups with respect to PSA, PSL, and LED. By the paraspinal approach, S1PS could be placed not only with a more medial orientation but also with a longer screw purchase than by the midline approach. In addition, the analysis showed that in the paraspinal approach group the S1PS pierced the anterior sacral cortex closer to the midline compared with the midline approach group (Figures 3A, B).

With respect to the anatomic location of the CIV, our results show that the MVD on the left side was significantly shorter than that on the right side. In contrast, our results show no significant difference in the SVD between the left and right sides (Table 3). Of 26 screws in the midline approach group, 4 left screws (15.4%) were vi-

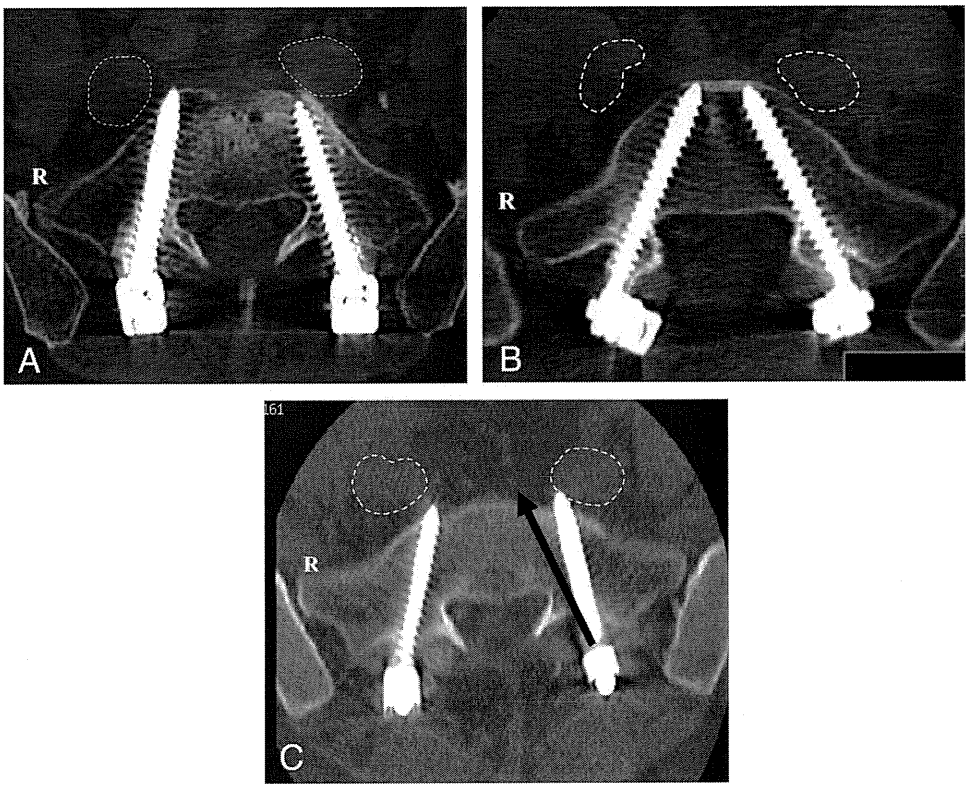

Figure 3. Three representative cases illustrated on postoperative CT images. The dotted circles show the contours of the CIV. **A,** An example of the placement in the midline approach group. IPD: 28.5/29.0 mm; PSA: 11.5/15.5 degrees; PSL: 47.5/46.0 mm; LED: 21.0/16.5 mm (right and left side, respectively). **B,** An example of the placement in the paraspinal approach group. IPD: 29.0/31.0 mm; PSA: 24.0/28.5 degrees; PSL: 55.0/54.0 mm; LED: 10.0/9.5 mm (right and left side, respectively). **C,** An example from the midline approach group where the S1PS lies adjacent to the CIV. MVD: 23.0/20.0 mm and SVD: 5.5/3.5 mm (right and left side, respectively). The left S1PS is evidently in contact with the left CIV. The ideal orientation of the left screw is indicated by the black arrow.

sually in contact with the left CIV (Figure 3C). On the other hand, no screw lay adjacent to the CIV in the paraspinal approach group (Table 4).

■ Discussion

In recent years, the Wiltse *et al* paraspinal approach to the lumbar spine,[20] which was achieved by developing the plane between the multifidus and the longissimus muscles, has been revised owing to an increased enthusiasm for development of minimally invasive operating techniques.[21,22] Several studies suggest that this procedure minimizes the ischemia and denervation of the paraspinal musculature resulting from the detachment of muscle from the spinous processes and its subsequent prolonged wide retraction used in the conventional midline approach, which may lead to postoperative muscle atrophy and pain.[23,24] Moreover, this procedure easily establishes access to the lateral aspect of the L5/S1 facet joint with minimal retraction of paravertebral muscles, although a few of the most lateral fibers of the multifidus are occasionally dissected because their bulky fibers are fanning caudally over the sacrum.[25]

Table 3. Location of the CIV

	Right Side	Left Side	*P*
MVD (mm)	23.6 ± 5.03	19.5 ± 8.33	0.0069*
SVD (mm)	6.99 ± 4.32	5.96 ± 5.27	0.1403

*$P < 0.05$.
MVD indicates the shortest distance from the midline to the CIV; SVD, the shortest distance from anterior sacral cortex to the CIV.

The present study demonstrated that it was possible to expose the optimal S1PS starting point located at the inferolateral corner of L5/S1 facet joint by both the midline and paraspinal approaches. However, in our series, the paraspinal approach provided a more medial orientation of S1PS placement. Although the midline approach managed to expose the entry point with wide retraction of the paravertebral muscles, it is likely that several factors would impede an ideal medially oriented placement of S1PS. It was pointed out that potential obstructions included a large screw head and shaft or wide instrumentation device, the prominence of the posterior iliac crest, muscle mass, and retractors.[26] Many authors have asserted that it is difficult to achieve a sufficiently medially oriented placement for the S1PS because of the dorsal overhang of the posterior iliac crest.[7,27,28,29] Kaptanoglu *et al* recommended first resecting the ilium to allow for a more medial trajectory for S1PS placement.[27] In the present study, the removal of the posterior superior iliac spine was not performed. Nevertheless, in the paraspinal approach group the reduction of the muscle volume impinging between the retractor and the posterior iliac crest enabled us to insert a screw with adequate medial orientation (Figure 4). From these

Table 4. No. Screws Contact With CIV

	Right Side	Left Side
Midline approach group (n = 26)	0	4 (15.4%)
Paraspinal approach group (n = 30)	0	0

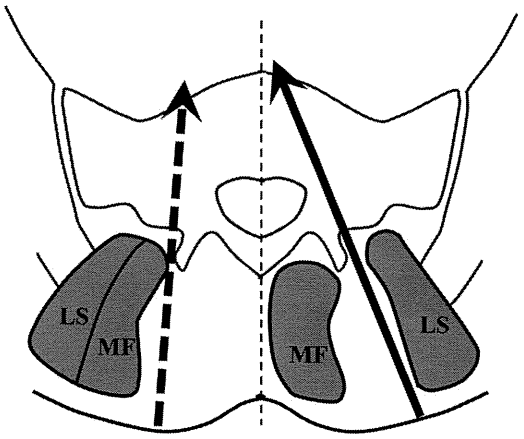

Figure 4. Schematic illustration of S1PS trajectory comparing the paraspinal and midline approaches. The arrow and dotted arrow represent the S1PS directions achieved by the paraspinal and midline approaches, respectively. MF indicates the multifidus muscle; LS, the longissimus muscle.

discussions, we stress that the paraspinal approach is particularly useful for S1PS placement in patients with either a bulky paravertebral muscle volume or a large overhang of the posterior iliac crest observed on preoperative CT or magnetic resonance imaging.

Medially oriented screw placement provides a more secure anchor to the sacrum for the 2 reasons mentioned in the Introduction, that is, the triangulation effect and the insertion of screws into denser bone. Our results, furthermore, demonstrated that the paraspinal approach gave a longer screw fixation than the midline approach, probably because of more medially oriented screw placement. Krag *et al* suggested that even a 5-mm longer screw can provide a significant increase in bone-screw fixation strength.[30] Several other biomechanical studies have generally supported the advantages of using a longer screw for S1.[8,28] Therefore, it can be concluded that S1PS placement through the paraspinal approach has several advantages from a biomechanical point of view.

So far as biomechanical advantages are concerned, bicortical fixation of S1PS has also been proved stronger.[10,13] Anatomic constraints, however, should be considered in the case of bicortical fixation. Several authors have recommended that placement of S1PS with a straight-ahead position should be avoided because it carries risks of damage to the iliac vessels, sympathetic chain, and the lumbosacral trunk that are closely applied to the sacrum.[16–19] In the present study, it was confirmed using the measurement of SVD that the interval between the CIV and the anterior sacral cortex was quite short. Therefore, we should be careful not to insert an overlong screw. However, based on the anatomic study by Mirkovic *et al*, it may be safe for a screw to penetrate the anterior sacral cortex within 22 mm of the midline.[16] These authors did not, however, refer to the difference in the anatomic location of the right and left common iliac vessels. Licht *et al* mentioned that the left CIV was at high risk at the S1 level because of the orientation of the vein across the anterior body of S1 after diverging from the inferior vena cava.[19] In the present study, the shortest distance from the midline to the left CIV (mean MVD; 19.5 mm), was indeed found to be significantly less than that to the right CIV (mean MVD 23.6 mm). This implies that the safe zone on the left side, at least for Japanese patients, is an even narrower range than Mirkovic *et al* suggested. According to the evaluation of LED, the S1PS tip in the midline approach pierced through an anterior sacral cortex laterally further from the midline than in the paraspinal approach. The fact that the mean value of LED (18.9 mm) in the midline approach was remarkably close to the left MVD (19.5 mm) is worthy of note. The present results indicate that there is a risk of injury to the left CIV in case of a bicortical S1PS placement in particular by the midline approach. Four left screws (15.4%) in the patients treated with the midline approach actually made contact with the left CIV, whereas no screw did in the paraspinal approach group. We emphasize that the medially oriented S1PS placement obtained with the paraspinal approach is very useful from the viewpoint of safety as well as mechanical strength.

There are some limitations in this study that deserve mention. First, major one is that this study had a retrospective design, with historical controls. The type of PS, the CT scanner, the surgeon, and the anatomy of the patients were not standardized. However, even under the blind prospective study, the surgeon-related bias does not become negligible because the surgeons would probably handle the PS angle intentionally if they know the purpose of the study in advance. To control the experimental condition and to reduce the bias, *in vitro* study using cadaver may be applicable. Second, the long-term outcomes of the 2 groups regarding instrumentation failure, bone union at the level of fusion, and clinical results were not investigated. Last, when it was difficult to accurately determine the rim of the CIV as described above, we were forced to exclude several cases.

■ Conclusion

To our knowledge, the current study is the first report that compares the paraspinal muscle-splitting approach with the conventional midline approach for S1PS placement. Our results demonstrate that the former may be superior to the latter with more medially oriented S1PS placement, which will provide stronger and safer fixation.

■ Key Points

- The positions of S1 pedicle screws inserted by a paraspinal approach were compared with those inserted using a midline approach using postoperative CT images along the screw axis.

- The paraspinal approach can lead to more medially oriented S1 pedicle screw placement than the midline approach, which should provide stronger fixation.
- Medially oriented S1 pedicle screw placement can be performed with less risk to the iliac vein, particularly on the left side, even with bicortical fixation.

References

1. Beguiristain JL, Martinez-Peric R, Barrios RH, et al. Lumbosacral arthrodesis with Louis technique. *Eur Spine J* 1994;3:169–71.
2. Ogilvie JW, Schengel M. Comparison of lumbosacral fixation devices. *Clin Orthop Relat Res* 1986;203:120–5.
3. Jackson RP, Hamilton AC. CD screws with oblique canal for improved sacral fixation: a prospective clinical study of the first fifty patients. In: *Seventh Proceeding of the International Congress on Cotrel-Dubousset Instrumentation*. Montpellier, France: Sauramps Medical; 1990:75–86.
4. Emami A, Deviren V, Berven S, et al. Outcome and complications of long fusions to the sacrum in adult spine deformity: luque-galveston, combined iliac and sacral screws, and sacral fixation. *Spine* 2002;27:776–86.
5. Devlin VJ, Boachie-Adjei O, Bradford DS, et al. Treatment of adult spinal deformity with fusion to the sacrum using CD instrumentation. *J Spinal Disord* 1991;4:1–14.
6. Carlson GD, Abitbol JJ, Anderson DR, et al. Screw fixation in the human sacrum: an in vitro study of the biomechanics of fixation. *Spine* 1992; 17(Suppl):S197–203.
7. Peretti F, Argenson C, Bourgeon A, et al. Anatomic and experimental basis for the insertion of a screw at the first sacral vertebra. *Surg Radiol Anat* 1991;13:133–7.
8. Lehman RA, Kuklo TR, Belmont PJ Jr, et al. Advantage of pedicle screw fixation directed into the apex of the sacral promontory over bicortical fixation. *Spine* 2002;27:806–11.
9. Von Strempel A, Trenkmann S, Kronauer I, et al. The stability of bone screws in the so sacrum. *Eur Spine J* 1998;7:313–20.
10. Zindrick MR, Wiltse LL, Widell EH, et al. A biomechanical study of intrapeduncular screw fixation in the lumbosacral spine. *Clin Orthop Relat Res* 1986;203:99–111.
11. Ruland CM, Mcafee PC, Warden KE, et al. Triangulation of pedicular instrumentation: a biomechanical analysis. *Spine* 1991;16(6 Suppl):S270–6.
12. Smith SA, Abittbol JJ, Carlson GD, et al. The effects of depth of penetration, screw orientation, and bone density on sacral screw fixation. *Spine* 1993;18: 1006–10.
13. Zheng YZ, Lu WW, Zhu Q, et al. Variation in bone mineral density of the sacrum in young adults and its significance foe sacral fixation. *Spine* 2000; 25:353–7.
14. Barber JW, Boden SD, Ganey T, et al. Biomechanical study of lumbar pedicle screws: does convergence affect axial pullout strength? *J Spinal Disord* 1998; 11:215–20.
15. Luk KD, Chen L, Lu WW. A stronger bicortical sacral pedicle screw fixation through the S1 endplate. *Spine* 2005;30:525–9.
16. Mirkovic S, Abitbol JJ, Strinman J, et al. Anatomic consideration for sacral screw placement. *Spine* 1991;16(6 Suppl):S289–94.
17. Esses SI, Botsford DJ, Huller RJ, et al. Surgical anatomy of the sacrum. A guide for rational screw fixation. *Spine* 1991;16(6 Suppl):S283–8.
18. Ergur I, Akcali O, Kiray A, et al. Neurovascular risks of sacral screws with bicortical purchase: an anatomical study. *Eur Spine J* 2007;16:1519–23.
19. Licht NJ, Rowe DE, Ross LM. Pitfalls of pedicle screw fixation in the sacrum. A cadaver model. *Spine* 1992;17:892–6.
20. Wiltse LL, Bateman JG, Hutchison RH, et al. The paraspinal sacrospinalis-splitting approach to the lumbar spine. *J Bone Joint Surg* 1968;50:919–26.
21. Vialle R, Wicart P, Drain O, et al. The Wiltse paraspinal approach to the lumbar spine revisited. *Clin Orthop Relat Res* 2006;445:175–80.
22. Foley KT, Holly LT, Schwender JD. Minimally invasive lumbar fusion. *Spine* 2003;28:26–35.
23. Hyun SJ, Lim YB, Kim YS, et al. Postoperative changes in paraspinal muscle volume: comparison between paramedical interfacial and midline approaches for lumbar fusion. *J Korean Med Sci* 2007;22:646–51.
24. Datta G, Gnanalingham KK, Peterson D, et al. Back pain and disability after lumbar laminectomy: is there a relationship to muscle retraction? *Neurosurgery* 2004;54:1413–20.
25. Weaver EN Jr. Lateral intramuscular planar approach to the lumbar spine and sacrum. *J Neurosurg Spine* 2007;7:270–3.
26. Robertson PA, Plank LD. Pedicle screw placement at the sacrum: anatomical characterization and limitations at S1. *J Spinal Disord* 1999;12:227–33.
27. Kaptanoglu E, Okutan O, Tekdemir I, et al. Closed posterior superior iliac spine impeding pediculocorporeal S-1 screw insertion. *J Neurosurg* 2003;99: 229–34.
28. Asher MA, Strippgen WE. Antrhopometric studies of the human sacrum relating to dorsal transsacral implant. *Clin Orthop Relat Res* 1986;203: 58–62.
29. Xu R, Ebraheim NA, Mohamed A, et al. Anatomic considerations for dorsal sacral plate-screw placement. *J Spinal Disord* 1995;8:352–6.
30. Krag MH, Beynnon BD, Pope MH, et al. Depth of insertion of transpedicular vertebral screws into human vertebrae: effect upon screw-vertebra interface strength. *J Spinal Disord* 1989;1:287–94.

Reinforcement of tendon attachment to bioactive porous titanium by BMP-2-induced ectopic bone formation

Kazutaka So,[1] Mitsuru Takemoto,[1] Shunsuke Fujibayashi,[1] Masashi Neo,[1] Tadashi Kokubo,[2] Takashi Nakamura[1]

[1]*Department of Orthopaedic Surgery, Graduate School of Medicine, Kyoto University, 54 Shogoin-kawahara-cho, Sakyo-ku 606-8507, Kyoto, Japan*

[2]*Department of Biomedical Sciences, College of Life and Health Sciences, Chubu University, 1200 Matsumoto-cho, Kasugai 487-8501, Aichi, Japan*

Received 21 April 2008; revised 25 July 2009; accepted 26 August 2009
Published online 12 November 2009 in Wiley InterScience (www.interscience.wiley.com). DOI: 10.1002/jbm.a.32640

Abstract: Achieving a firm attachment between a tendon and a metal remains a major challenge in orthopedic surgery. In this study, we developed a simple model for evaluating the strength of this attachment using bioactive porous titanium, and confirmed whether bone morphogenic protein-2 (BMP-2) can be a help in achieving a firm attachment by ectopic bone formation. Rectangular plate-shaped implants were soak-loaded with BMP-2 (B+ group) and were implanted within the patellar tendon of a rabbit. Implants without BMP-2 (B− group) were used as controls, and they were harvested at 4 and 8 weeks postoperation for mechanical tests and for histological and histomorphometric study. The pull-out failure load of the B+ group was significantly higher than that of the B− group and new bone was more prevalent within the pores and around the implants in the B+ group than in the B− group. The model used in this study was feasible for evaluating the tendon–metal attachment, and a combination of bioactive porous titanium and BMP-2 was found to attach firmly to the tendon. © 2009 Wiley Periodicals, Inc. J Biomed Mater Res 93A: 1410–1416, 2010

Key words: tendon; titanium; BMP (bone morphogenic protein); mechanical test; drug delivery

INTRODUCTION

In prosthetic surgeries involving malignant bone tumors and comminuted fractures of the proximal humeral bone, firm attachment between the tendon and the metal prosthesis is necessary to enhance joint stability and control of the limb. However, the solution to this challenge has not been realized[1,2] because tendon tissue is poor in vascularity and healing ability,[3,4] and the prosthesis is poorer still. To solve this problem, a new material and a new method have been proposed in previous papers.[5–9] Some of these studies show that the attachment can be reinforced by interposing bone between the tendon and the metal. For this method to be successful, bone should not only be interposed, but also attach firmly to both the tendon and the metal *in vivo*.

Correspondence to: K. So; e-mail: so_kazu@kuhp.kyoto-u.ac.jp

Interposed bone has been mainly supplied by autograft or allograft in the previous studies.[6–9] However, bone grafting does not solve all problems such as donor site morbidity, additional required procedures, and the long time required for the grafted bone to be revascularized. For simplicity and reproducibility in this study, we used bone morphogenic protein-2 (BMP-2) to interpose new bone between the tendon and the metal.

Bioactive-treated titanium has been previously demonstrated to attach directly to the bone[10,11] and to have excellent osteoconductivity and osteoinductivity *in vivo*.[12–14] Bioactive porous titanium was tested here as a promising metal that can firmly attach to the tendon via interposed bone.

This study aimed to confirm whether direct and firm attachment between the tendon and the bioactive porous titanium could be formed via bone with addition of BMP-2. A simple experimental model using rabbit patellar tendon was developed to evaluate the attachment. In the model, histological investigations and mechanical tests were performed to evaluate the osteoinductivity of the implant and the pull-out strength of the tendon/implant complex, respectively.

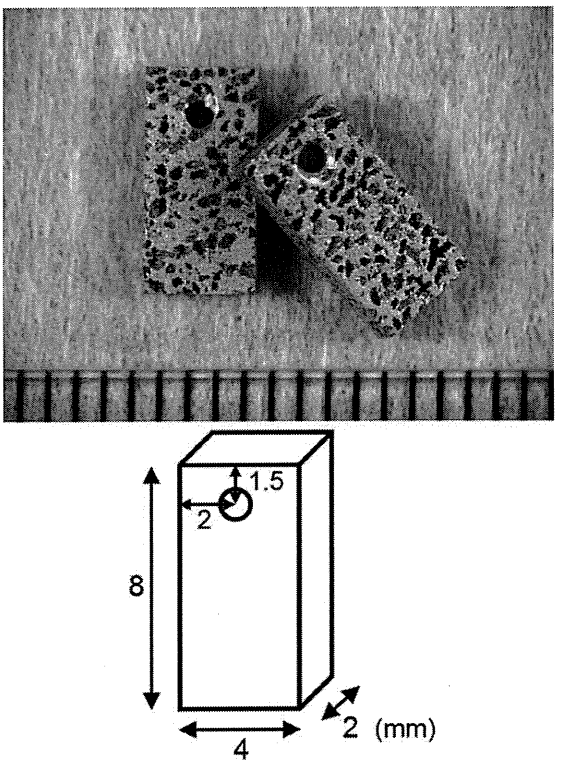

Figure 1. Photograph and design drawing of porous titanium implants used in this study. [Color figure can be viewed in the online issue, which is available at www.interscience.wiley.com.]

MATERIALS AND METHODS

Preparation of porous titanium

Sintered porous titanium implants (porosity 50%; average pore size ± standard deviation 303 ± 152 μm) were supplied by Osaka Yakin Co., Ltd (Japan) and were manufactured through sintering of titanium powders added with volatile spacer particles (ammonium hydrogen carbonate) as previously described.[14–17] For animal experiments, rectangular plate-shaped implants (4 mm × 8 mm × 2 mm) were cut from the sintered body using electric-discharge machining, and a hole (1 mm in diameter) was made on each implant (Fig. 1).

Bioactive surface treatment and loading of BMP-2

For bioactive treatments, the titanium substrates were immersed in aqueous 5*M* NaOH solution at 60°C for 24 h, 0.5 m*M* HCl at 40°C for 24 h, ultrapure water at 40°C for 24 h, and then heat-treated at 600°C for 1 h, as previously described.[14,17] The homogeneity of the bioactive surface was confirmed by examining the topography and composition of the center and peripheral parts of several implants using a scanning electron microscope (SEM), an energy dispersive X-ray microanalyzer connected to the SEM, and X-ray diffractometry. *In vitro* apatite-forming ability was confirmed by soaking samples in simulated body fluid[18] for 3 d.

After sterilization in ethylene oxide, half of the implants were soak-loaded with 5 μg of recombinant human BMP-2 (Astellas Pharma Inc., Japan) and were freeze-dried before surgery.

Animal experiments

Sixteen Japanese white male rabbits weighing between 2.7 and 3.0 kg underwent operations. Intravenous injection of pentobarbital sodium (70 mg/kg) and local administration of 0.5% lidocaine (20 mg) was used for anesthesia. Animals were placed in a supine position, and the bilateral patellar tendon was exposed in an aseptic manner. A slit was made in the coronal plane to divide it into anterior and posterior halves, and an implant was inserted into the tendon slit with its hole located proximally [Fig. 2(a)]. Eight animals received 16 implants without BMP-2 (B− group), and eight animals received 16 implants loaded with BMP-2 (B+ group). After implantation, the bilateral edge of each tendon was sutured to prevent implant migration and also to seal the implant within the tendon tissue. The animals were kept individually in cages without immobilization until euthanasia.

Four animals in each group were euthanized with intravenous pentobarbital sodium at 4 weeks postoperation, and the remaining animals were euthanized after 8 weeks. Thus, eight samples from each group were harvested for each implantation period. Six were used for quantitative evaluation using mechanical tests and histomorphometric analyses. The remaining two samples were used to represent the typical histology of each group. This animal study

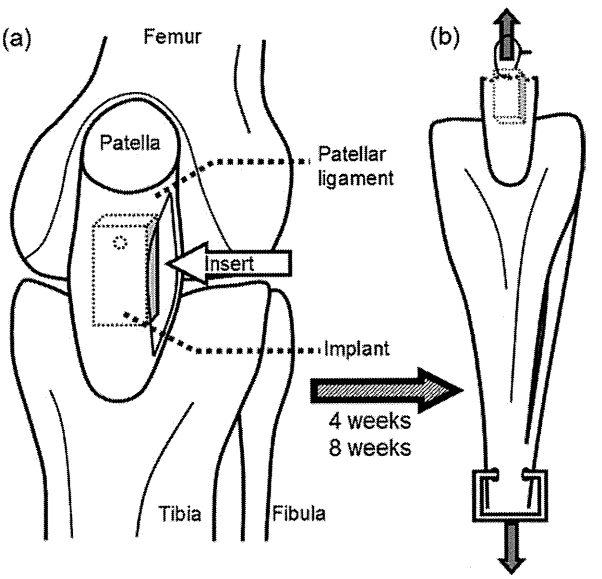

Figure 2. Schematic diagram of experimental methods. (a) A porous titanium implant was inserted into the slit of tendon. (b) Mechanical tests were performed to evaluate the pull-out failure load at 4 and 8 weeks after surgery.

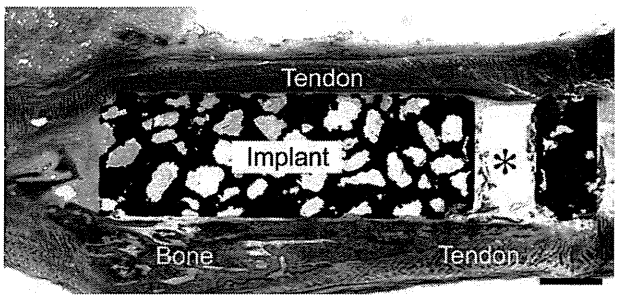

Figure 3. Calculation of bone coverage rate. Bone coverage rate (%) = (length of yellow dot line)/(length of white dot line) × 100. * The hole that wire was passed through for the mechanical test. The bone coverage rate was measured on the area distal to the hole. Scale = 1 mm. [Color figure can be viewed in the online issue, which is available at www.interscience.wiley.com.]

was approved by the Animal Research Committee, Graduate School of Medicine, Kyoto University, Japan.

Mechanical tests

Patellar tendons, including the implant, and tibial bone were harvested *en bloc* for evaluation of the attachment strength between the implant and the tendon. The implant surface proximal to the hole was exposed, and a 24G soft wire ~20 cm in length was inserted into the hole and was looped. The pull-out failure load of the tendon/implant complex was measured by pulling the soft wire and a hook attached to the distal end of tibia at a cross-head speed of 35 mm/min [Fig. 2(b)]. The failure load (*N*) was recorded using an Instron-type autograph (Model 1011, Aikoh Engineering Co., Ltd, Japan), and the results are presented as mean ± standard deviation.

Histomorphometric and histological analyses

After the mechanical tests, the implants were reduced into the tendons, and the tendons were resected from the tibiae at the insertion. Specimens were fixed in 10% phosphate-buffered formalin, dehydrated in ethanol at serial concentrations, and embedded in polyester resin. Sections 500 μm in thickness were cut with a band saw (Microcutting machine BS-3000S, EXACT, Germany) in the sagittal plane. The middle sections were ground to a 40 μm thickness using a grinding-sliding machine (Microgrinding machine MG-4000, EXACT, Germany) and stained with Stevenel's blue and Van Gieson's picrofuchsin. They were observed by light microscopy (Eclipse 80i, Nikon, Japan) and fluorescence microscopy (IX70, Olympus, Japan), and were recorded with digital cameras. Histomorphometric analyses were performed on the area distal to the hole using Adobe Photoshop 6.0 (Adobe Systems Inc., USA) and ImageJ (National Institutes of Health, USA). The bone area around and within the implant (mm^2) was separately measured using fluorescence microphotographs.[16] Bone coverage rate (%) was defined as the percentage of length of implant surface covered with bone or cartilage to length of total implant surface (Fig. 3). Using Statcel software,[19] the results were analyzed statistically by an unpaired *t*-test. Differences with a $p < 0.05$ were considered statistically significant.

For histological observation, implants were harvested with surrounding tendon tissue after euthanasia and were not subjected to mechanical testing. After being embedded in polyester resin, they were sectioned, ground, stained, and recorded in the same way.

RESULTS

Mechanical tests

Results of the mechanical tests are summarized in Figure 4. The pull-out failure load of the B− and B+ groups were 9.3 ± 2.7 *N* and 25.1 ± 8.4 *N* at 4 weeks ($n = 6$, $p < 0.005$); and 12.9 ± 3.2 *N* and 142.4 ± 33.9 *N* at 8 weeks ($n = 6$, $p < 0.0001$), respectively. Macroscopically, implant failure did not occur during the mechanical test. Failure occurred mostly at the interface between the implant and the surrounding tissue or within the bone. Tendinous tissue was rarely found to remain on the outer surface of the implants.

Histological and histomorphometric analyses

In the B− group, no new bone was histologically found at the interface between the tendon and the implant, and the two elements appeared to be attached directly to each other [Fig. 5(a)]. A tiny bone was found within a pore in one B− sample after 8 weeks [Fig. 5(b)]. On the other hand, new bone was abundantly found in the B+ group. After 4 weeks, bone formed mainly around the implants and rarely within the pores [Fig. 6(a)]. After 8 weeks,

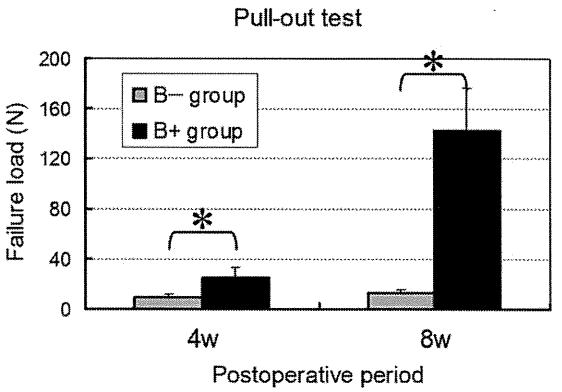

Figure 4. Results of the mechanical test. Differences between values of the B− group and the B+ group were significant at both postoperative periods (*$p < 0.05$).

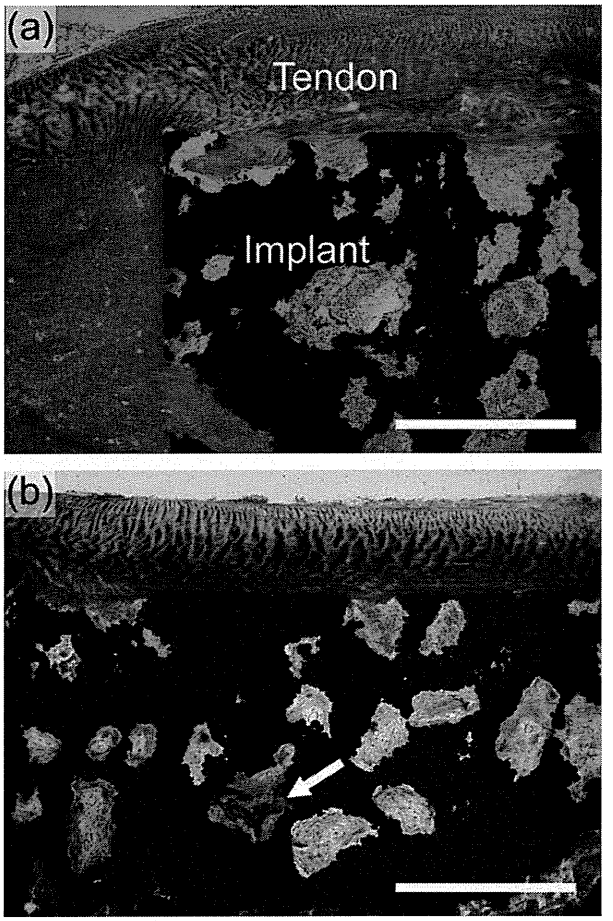

Figure 5. Histology of the B− group. (a) Sample without mechanical test; (b) after mechanical test. No new bone was found around the implants (a). A tiny new bone was found within a pore in one sample after 8 weeks (b, arrow). Scale = 1 mm. [Color figure can be viewed in the online issue, which is available at www.interscience. wiley. com.]

new bone was found also within the pores and was in contact with the inner surface of the implant [Fig. 6(b)]. Although direct attachment between the bone and the outer surface of the implant was rare after only 4 weeks, it was common after 8 weeks. At 8 weeks, new bone contained marrow-like tissue and appeared more mature than at 4 weeks.

At the tendon–bone interface, fibrocartilage cells were found in some places [Fig. 7(a)]. They were embedded in both mineralized and unmineralized matrices, and were arranged in rows parallel to the direction of the tendon fibers. Dense collagen fibers were also found at the tendon–bone interface [Fig. 7(b)]. They were arranged perpendicular to the interface and parallel to the direction of the tendon fibers.

Bone area around the implant in the B− group and the B+ group was 0 ± 0 and 2.6 ± 1.6 mm^2 at 4 weeks (n = 6) and 0 ± 0 and 6.0 ± 3.1 mm^2 at 8 weeks [n = 6, Fig. 8(a)], respectively. Bone area within the implant pores was 0 ± 0 and 0.039 ± 0.058 mm^2 at 4 weeks (n = 6) and 0.0075 ± 0.018 and 1.1 ± 0.45 mm^2 at 8 weeks [n = 6, Fig. 8(a)], respectively. Bone coverage rates of the two groups were 0 ± 0 and 54.9 ± 18.2% at 4 weeks (n = 6) and 0 ± 0 and 73.5 ± 18.4% at 8 weeks [n = 6, Fig. 8(b)], respectively.

DISCUSSION

A simple experimental model was established in this study to evaluate the attachment between the tendon and the metal histologically and mechani-

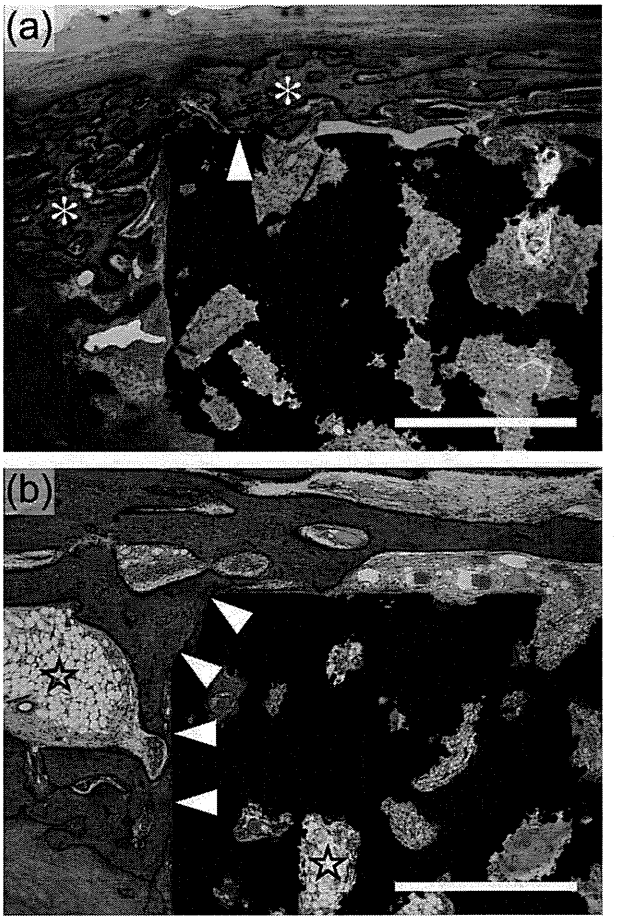

Figure 6. Histology of the B+ group. New bone was formed around the implants (asterisk), but was rarely found within pores after only 4 weeks (a). Increasing amounts of new bone were found both around and within implants after 8 weeks (b). Newly formed bone appeared to be more mature with marrow-like tissue (star), and have a greater area of direct attachment with the outer surface of implants (arrow head) at 8 weeks than at 4 weeks. Scale = 1 mm. [Color figure can be viewed in the online issue, which is available at www.interscience.wiley.com.]

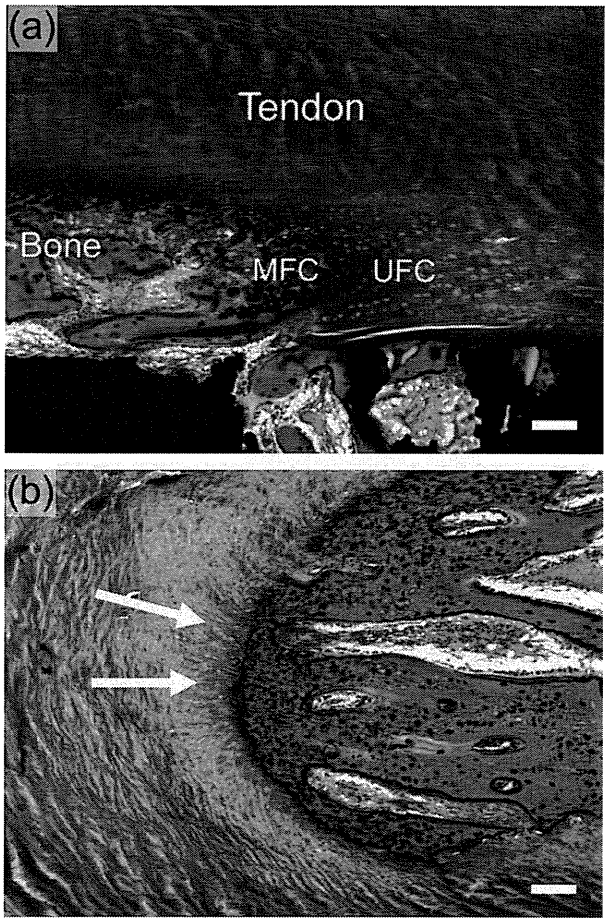

Figure 7. Histology of bone–tendon interface. Mineralized fibrocartilage (MFC) and unmineralized fibrocartilage (UFC) lie between bone and tendon (a). Dense collagen fibers (arrow) were found at the interface between bone and tendon (b). Scale = 100 μm. [Color figure can be viewed in the online issue, which is available at www.interscience.wiley.com.]

cally. Although the initial fixation and the implanting method of the current model did not imitate clinical conditions, the results were reproducible and reliable. Our findings clearly show that bioactive porous titanium can attach directly and firmly to tendon via ectopically formed bone when BMP-2 is supplemented. In comparison with experimental models in previous studies of tendon attachment to metal,[5–9] our model was more feasible in that implant preparation and operative methods were simple and easy, the experimental period was short, and animal welfare was of high priority.

Histologically, no new bone was found within or around implants of the B− group except in one sample, and the implants were totally surrounded by tendon or scar tissue (Fig. 5). According to previous reports, it took at least 3 months to confirm ectopic bone formation within the pores of the bioactive porous titanium in the back muscle of beagle dogs,[14] and ectopic bone formation could rarely be observed in rodents.[20,21] It is reasonable that almost no new bone was found after only 8 weeks in this study. Although the tendon was histologically in direct contact with the outer surface of the implant, their interface was revealed to be weak by mechanical testing.

On the other hand, new bone was significantly formed in the B+ group not only within pores of implants, but also around them (Figs. 5, 6, 8a), and the pull-out strength of the tendon/implant complex was successfully reinforced. Interestingly, new bone formation was more vigorous around the implant than within the pores (Figs. 6, 8a). These findings support that the *in vivo* environment around the implant was more preferable for new bone formation than that within the pores. It is our speculation that precursor cells and matrices available for new bone formation were more abundant around the implant. The most meaningful finding in this study is that simple loading of BMP-2 can result in reinforcing tendon attachment to bioactive porous titanium.

It is remarkable that ectopic bone was efficiently formed, although no degradable carrier for the con-

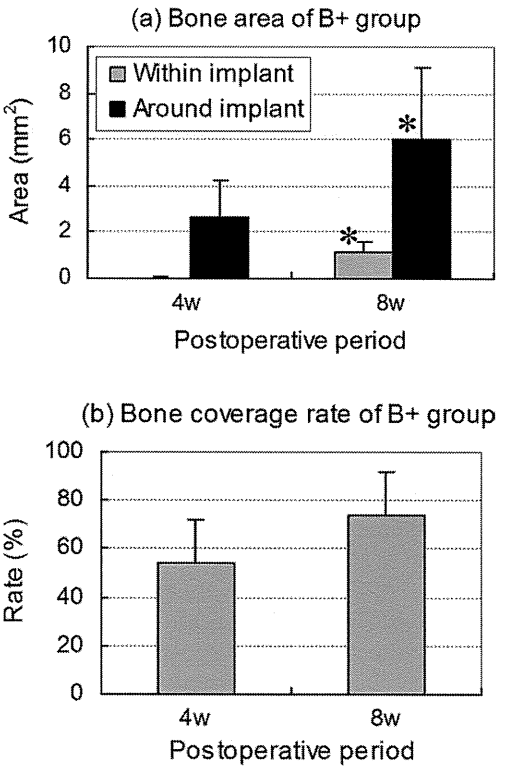

Figure 8. Results of histomorphometry of B+ group. (a) New bone area within and around the implant significantly increased during the observation period (*$P < 0.05$). (b) Bone coverage rate also increased during the observation period. The rate at 4 and at 8 weeks was different ($P = 0.095$).

trolled release of BMP-2 was used in this study. In our preliminary study, it was found that BMP-2 was poorly released from the implant *in vitro*. The bioactive-treated surface may have a high affinity for BMP-2. In general, a local and controlled delivery system is necessary for ectopic bone formation by BMP-2.[22] Collagen impregnation and hydroxyapatite coating are popular methods for controlled release of agents from metallic materials.[23] However, they have disadvantages such as disease transmission, alteration to macropore topography, and delamination *in vivo*.[24] We demonstrate that bioactive porous titanium does not require such additional treatment for new bone formation by BMP-2.

Histologically, fibrocartilage and dense collagen fibers were found at the tendon–bone interface in the B+ group (Fig. 7). Because failure at this interface was not found by the pull-out test, we speculate that this interface's strength may result from regeneration of biological enthesis-like structures.[7,25] The overall strength of the tendon/implant complex depended on the strength of the bone–implant interface and of the bone itself, corresponding to mechanical test failure in that area. The area of direct attachment between the bone and the implant increased as the bone matured (Fig. 6). As well as bone volume and coverage rate, the maturity of the bone was considered to influence the bone–implant interface.

Yamamoto et al. reported that 34 μg of BMP-2/cm^3 of hydrogel was sufficient to enhance bone regeneration.[26] According to their study, the required dose of BMP-2 in our model was only 2.176 μg/implant. However, we found that 3 μg of BMP-2/implant was insufficient for new bone formation in our preliminary study, and decided to use 5 μg/implant in this study.

The experimental model used in this study has some limitations, for instance that the initial fixation does not imitate clinical conditions. However, it would be beneficial to conduct further research into the method of forming firm attachments quickly using this simple and easy model. For example, grafting bone chips or artificial bone granules around the BMP-2-loaded implant could improve the results, because it would provide substrates and void spaces for bone formation. A combination of BMPs and allogenic bone graft has already been shown to have synergic effects on bone formation.[9,27] In addition, modification of the bioactive treatment would influence the attachment strength by several mechanisms. It would vary the bioactivity of the implant surface, the attachment strength per unit area,[10] and the drug release profile. Additional studies using the current model will discover better materials and methods to form a firm attachment rapidly before moving into clinical studies.

CONCLUSIONS

An experimental model was established in this study to evaluate the attachment between the tendon and the metal. Our findings show that attachment between the bioactive porous titanium and the tendon can be significantly reinforced by BMP-2-induced ectopic bone formation. We expect that a simple combination of bioactive porous titanium and BMP-2 will contribute to a better joint function when used in the metal prosthesis.

References

1. Damron TA. Endoprosthetic replacement following limb-sparing resection for bone sarcoma. Semin Surg Oncol 1997;13:3–10.
2. Frankle MA, Mighell MA. Techniques and principles of tuberosity fixation for proximal humeral fractures treated with hemiarthroplasty. J Shoulder Elbow Surg 2004;13:239–247.
3. Ahmed IM, Lagopoulos M, Mcconnell P, Soames RW, Sefton GK. Blood supply of the Achilles tendon. J Orthop Res 1998;16:591–596.
4. Fenwick SA, Hazleman BL, Riley GP. The vasculature and its role in the damaged and healing tendon. Arthritis Res 2002;4:252–260.
5. Reach JS, Dickey ID, Zobitz ME, Adams JE, Scully SP, Lewallen DG. Direct tendon attachment and healing to porous tantalum: An experimental animal study. J Bone Joint Surg Am 2007;89:1000–1009.
6. Gottsauner-Wolf F, Egger EL, Giurea A, Antosch M, Olsen D, Rock MG, Sim FH. Biologic attachment of an allograft bone and tendon transplant to a titanium prosthesis. Clin Orthop Relat Res 1999;101–110.
7. Inoue N, Ikeda K, Aro HT, Frassica FJ, Sim FH, Chao EY. Biologic tendon fixation to metallic implant augmented with autogenous cancellous bone graft and bone marrow in a canine model. J Orthop Res 2002;20:957–966.
8. Oddy MJ, Pendegrass CJ, Goodship AE, Cannon SR, Briggs TW, Blunn GW. Extensor mechanism reconstruction after proximal tibial replacement. J Bone Joint Surg Br 2005;87:873–878.
9. Higuera CA, Inoue N, Lim JS, Zhang R, Dimaano N, Frassica FJ, Chao EY. Tendon reattachment to a metallic implant using an allogenic bone plate augmented with rhOP-1 vs. autogenous cancellous bone and marrow in a canine model. J Orthop Res 2005;23:1091–1099.
10. Fujibayashi S, Nakamura T, Nishiguchi S, Tamura J, Uchida M, Kim HM, Kokubo T. Bioactive titanium: Effect of sodium removal on the bone-bonding ability of bioactive titanium prepared by alkali and heat treatment. J Biomed Mater Res 2001;56:562–570.
11. Nishiguchi S, Kato H, Fujita H, Oka M, Kim HM, Kokubo T, Nakamura T. Titanium metals form direct bonding to bone after alkali and heat treatments. Biomaterials 2001;22:2525–2533.
12. Fujibayashi S, Neo M, Kim HM, Kokubo T, Nakamura T. Osteoinduction of porous bioactive titanium metal. Biomaterials 2004;25:443–450.
13. Takemoto M, Fujibayashi S, Neo M, Suzuki J, Kokubo T, Nakamura T. Mechanical properties and osteoconductivity of porous bioactive titanium. Biomaterials 2005;26:6014–6023.
14. Takemoto M, Fujibayashi S, Neo M, Suzuki J, Matsushita T, Kokubo T, Nakamura T. Osteoinductive porous titanium